

Computational Design of Homotetrameric Peptide Bundle Variants Spanning a Wide Range of Charge States

*Rui Guo¹, Nairiti J. Sinha^{2,4}, Rajkumar Misra², Yao Tang², Matthew Langenstein², Kyunghee Kim², Jeffery A. Fagan³, Christopher J. Kloxin^{2,5}, **Grethe Jensen^{†4, 5}**, Darrin J. Pochan^{*2}, Jeffery G. Saven^{*1}*

¹Department of Chemistry, University of Pennsylvania, Philadelphia, PA, USA

²Department of Materials Science and Engineering, University of Delaware, Newark, DE, USA

³Materials Science and Engineering Division, National Institute of Standards & Technology (NIST), Gaithersburg, MD, USA

⁴NIST Center for Neutron Research (NCNR), National Institute of Standards & Technology (NIST), Gaithersburg, MD, USA

⁵Department of Chemical and Biomolecular Engineering, University of Delaware, Newark, DE, USA

† Present address: Danish Technological Institute, Tåstrup, Denmark

* Corresponding authors: poch@udel.edu, saven@sas.upenn.edu

KEYWORDS:

computational peptide design, supercharged proteins, protein electrostatic interactions, helical peptides, coiled coil, bundlemer, nanorods

Abstract

With the ability to design their sequences and structures, peptides can be engineered to realize a wide variety of functionalities and structures. Herein computational design was used to identify a set of 17 peptides having a wide range of putative charge states but the same tetrameric coiled-coil bundle structure. Calculations were performed to identify suitable locations for ionizable residues (D, E, K and R) at the bundle's exterior sites, while interior hydrophobic interactions are retained. The designed bundle structures span putative charge states of -32 to +32 in units of electron charge. The peptides were experimentally investigated using spectroscopic and scattering techniques. Thermal stabilities of the bundles were **investigated** using circular dichroism. Molecular dynamics simulations assessed structural fluctuations within the bundles. The cylindrical peptide bundles, 4 nm long by 2 nm diameter, were covalently linked to form rigid, micron-scale polymers and characterized using transmission electron microscopy. The **designed** suite of sequences provides a set of readily realized nanometer-scale structures of tunable charge that can also be polymerized to yield rigid-rod polyelectrolytes.

Introduction

In addition to their central importance to the molecular basis of life processes, protein- and peptide-based systems have a wide range of applications to therapeutics,¹⁻⁷ foods,⁸⁻¹⁰ catalysts¹¹⁻¹⁶ as well as nanoscale and macroscale materials.¹⁷⁻²⁵ Given that structure and function can often be encoded in the sequence of the amino acids, targeted properties can in principle be achieved *via*

careful selection of sequence, solution conditions, and processing. Peptides have been used to engineer a wide range of assemblies, including nanotubes, nanosheets, nanolattices and polymers of peptide building blocks.²⁶⁻³⁷ The structure, functionality, and aggregation of proteins are a result of multiple noncovalent interactions, including electrostatic effects, hydrogen bonding, and hydrophobic interactions. Deconvoluting and investigating these interactions can inform our understanding of the principles guiding protein behavior and enhance our capacity to engineer protein materials.

Electrostatic interactions, in particular, are fundamental to protein properties such as thermal stability, solubility, intermolecular association, enzymatic recognition, and colloidal behavior. There have been efforts to engineer large scale variation of charge *via* substitution of ionizable residues both to implement specific functionalities and to investigate the electrostatic effects of charges on protein association^{38, 39}. Recent efforts have focused on engineering supercharged variants of proteins,⁴⁰⁻⁴⁶ tuning the solubility of membrane proteins by modifying surface charges,⁴⁷⁻⁴⁹ creating uncharged or highly charge-depleted proteins,^{50, 51} and peptides containing only one type of charge.⁵² Complementary electrostatic charge has also been used to develop large, nanostructured assemblies from engineered protein building blocks.^{30, 31, 53} Linked chains of charged proteins have provided vehicles for studying polyelectrolyte properties with precisely engineered polymers.⁵⁴⁻⁵⁷ Engineering wide variation of charge states can be subtle, however, and substitutions can often yield unstructured or aggregation-prone sequences. As a result, methods that can address large variation in sequence are usually employed, such as directed evolution^{40, 42} and computational protein design.^{43-47, 58, 59}

Herein, using computational design, we explore the systematic tuning of the putative charge of a peptide while preserving the folded structure. Related studies have been pursued using variants

of natural proteins such as antibodies,⁴³ but herein we consider a short peptide sequence that folds upon oligomerization to present a targeted charge and set of exterior ionizable amino acid residues. *De novo* designed helical bundles are a promising candidate in this regard, as many stable coiled-coil structures of varying length have been reported.⁵⁹⁻⁶⁶ Additionally, helical peptide sequences can be rapidly synthesized, characterized, and chemically modified. Peptides can also be reversibly processed over a wide range of solution conditions, where manipulation of such conditions can confer hierarchical assembly to distinct material structures.⁶⁷⁻⁶⁹ Here, a probabilistic design approach^{56, 70-72} was applied to a *de novo* designed tetrahelical backbone,⁵⁹ to design variants of the peptide with distinct charge features. More specifically, each peptide variant has a unique putative charge state q for a single helix chain, and the whole series of bundles span from $q = -8$ to $q = +8$, q being the charge of the sequence expected at pH 7 in units of the electron charge. The resulting 17 designed sequences (**Table 1**) shared the same helical backbone and interior hydrophobic residues, with the bundles spanning a range of putative charges from $q = -32$ to $q = +32$. With appropriate N-terminal functionalization, related bundles have yielded polymers of unusually large persistence lengths, where the bundle serves as the monomeric building block.⁵⁶ The sequences were realized experimentally to assess: (a) the folding and assembly despite the net repulsive electrostatic interactions between chains for the 17 peptide bundles; (b) the alpha-helical content; (c) the thermal stabilities of sequences; (d) the oligomerization state of the bundles; and (e) the capacity to polymerize the bundles, where chemically functionalized bundles serve as monomer building blocks.

Materials and Methods

Computational Peptide Design

A probabilistic approach to peptide sequence design that has been described previously^{59, 70-73} was employed. For predetermined constraints on the sequences, the method estimated probabilities of the amino acids at variable positions within the bundle structure. The probabilities were then used to guide amino acid substitutions so as to achieve targeted charge states of the peptide. Constraints appeared as functions of the amino acid probabilities, and the specification of the overall charge was achieved by constraining the average charge over these probabilities.

$$q = \sum_i (q_+/e)(w_{i,Lys} + w_{i,Arg}) + (q_-/e)(w_{i,Glu} + w_{i,Asp}) \quad (1)$$

Here $q_+ = +e$ and $q_- = -e$, given that e is the charge on the electron, and $w_{i,a}$ is the probability of amino acid a at residue site i . The computational design process used the previously *de novo* designed structure and sequence of BNDL1,⁵⁹ a tetramer-forming sequence, as a starting point and structural template.

Molecular Dynamics Simulations

Molecular dynamics (MD) simulations were performed on each sequence to assess the peptide bundle's **structural fluctuations** in an aqueous solution. The computationally designed dimensions of the bundle were roughly (nm) $2.7 \times 2.7 \times 5.0$, and the peptide was solvated in a cubical water box with the edge length of 8.0 nm. Sodium and chloride ions were added to neutralize the net charge of the peptide and achieve an approximate net concentration of 0.15 M. The NPT (**constant number of particles N, temperature T and pressure P**) ensemble was employed with pressure of 0.1 MPa and temperature of 300 K. The CHARMM36 force field⁷⁴ and TIP-3P water model⁷⁵ were used. The system went through 50 steps of minimization and then 40 ns of MD simulation with a 2 fs time step. Solvent and counter ions were added using VMD 1.9.3.⁷⁶ Minimization and

simulation were done by NAMD 2.12.⁷⁷ Configurations sampled from the second half of the trajectory (20 ns to 40 ns) were used for structural analysis.

Peptide Synthesis Reagents

All amino acids, resin and activator were purchased from ChemPep and CEM and used as received. N, N-dimethylformamide (DMF), trifluoroacetic acid (TFA), triisopropylsilane (TIPS) and other reagents were purchased from Sigma-Aldrich. Final concentrations of all peptides were prepared from their respective stock solution as needed.

Peptide Synthesis

All peptide sequences were synthesized using standard solid-phase peptide synthesis methods on Rink Amide resin on a 100 μmol scale using a CEM Liberty Blue microwave-assisted automated peptide synthesizer. Standard Fmoc protection chemistry was employed in combination with coupling cycles comprising diisopropylcarbodiimide (DIC) and ethyl (hydroxyimino)cyanoacetate (Oxyma) mediated activation protocols and base-promoted deprotection using 20 % (by volume) piperidine in N, N-dimethylformamide under microwave conditions.^{56, 59} The peptides were cleaved from the resin using a cocktail solution comprising (by volume) 95 % trifluoroacetic acid (TFA), 2.5 % triisopropylsilane (TIPS), and 2.5 % Milli-Q water at room temperature for 3 h. Then the cleavage solution was filtered, and the volume reduced to \approx 5 mL under a flow of nitrogen. The crude peptides were precipitated in cold diethyl ether (40 mL) and centrifuged at 420 rad/s (4,000 rpm) for 10 min. The supernatant was then discarded, and the precipitate allowed to dry overnight, redissolved in water/acetonitrile (50:50 volume %, 5 mL) and lyophilized to yield a fine white solid.

Peptide Purification

All peptides were purified *via* reverse-phase high pressure liquid chromatography (HPLC) using a BEH130 Prep C18 10 μm column (XBridge, Waters Corporation, Milford, MA). Crude peptides were dissolved in Milli-Q water and filtered (0.20 μm filter, Corning, Inc., Corning, NY) before HPLC injection. A gradient of water (0.1 % TFA,) and acetonitrile (0.1 % TFA,) between 30 % and 70 % over 35 min at a flow rate 30 mL/minute was used. Pure fractions were combined and lyophilized. The purity was confirmed by analytical UPLC-MS (Waters Xevo G2-S QToF, Waters Corporation).

Circular Dichroism Spectroscopy

All peptide solutions were prepared at 100 μM concentration in 25 mM sodium phosphate buffer (pH 7). Each CD spectrum was baseline corrected and recorded as the average of 2 scans from 185 to 250 nm using a JASCO 815 (scanning speed 50 nm/min; bandwidth 1.0 nm) in 1 mm pathlength quartz cuvette. Temperature-dependent CD experiments were performed in the temperature range from 10 $^{\circ}\text{C}$ to 80 $^{\circ}\text{C}$ at a heating rate of 1 $^{\circ}\text{C}/\text{min}$, and peptide solutions were incubated for 2 min before measurement at each temperature. The molar ellipticity at 222 nm was monitored as a function of temperature.

Analytical Ultracentrifugation

Analytical ultracentrifugation (AUC) was conducted in a Beckman-Coulter XL-I analytical ultracentrifuge using a Ti-50 rotor and 12 mm cells with sapphire windows. Measurements were performed at 20.0 $^{\circ}\text{C}$ with concentrations of 100 - 200 μM peptide and 50 mM NaCl in a 400 μL

volume. A pre-spin equilibration of minimum of 2 h was performed to ensure temperature homogeneity. All measurements were conducted at 4400 rad/s (42 krpm). Radial absorbance scans were measured at 280 nm (~170 scans/cell/experiment). Analysis of the recorded radial absorbance profiles as a function of time was conducted using the numerical fitting software SEDFIT (V15.01b).⁷⁸ Sedimentation was modelled using the sedimentation coefficient $c(s)$ model where s is the sedimentation coefficient. Values for the molar mass M of each complex can be determined from the measured s -values using the equation:

$$M^{2/3} = \frac{s N_A f / f_0 6\pi\mu}{(1-\bar{v}\rho_s)} \left(\frac{3}{4\pi N_A} \bar{v} \right)^{1/3} \quad (2)$$

Here \bar{v} is the partial molar volume, N_A is Avogadro's constant, and f/f_0 is the ratio of the experimentally determined friction coefficient to that of a sphere of the same mass and density. The density (ρ_s) and viscosity (μ) of the aqueous solutions used for dilution of samples in the experiments were measured separately in an Anton-Parr DMA 5000 - LOVIS M densitometer-viscometer. AUC data analysis and fit parameters are included in the supplementary information (SI). Uncertainties reflect one standard deviation of the reported value.

Small-Angle Neutron Scattering (SANS)

SANS measurements were performed on CNHRN vSANS beamline at the National Institute of Standards and Technology (NIST) Center for Neutron Research (NCNR), National Institute of Standards and Technology, Gaithersburg, Maryland, USA. Default instrument configurations were utilized for the measurements. Samples were prepared by suspending lyophilized peptide in and subsequently dialyzing against deuterium oxide (D₂O, Sigma). The pD of the final solution was 5.5 as measured using a pH probe and adjusted for heavy water (pD = pH +0.4). The scattering intensity curve $I(Q)$ was fit to a cylinder form factor model as described previously.⁷⁹ Here, the

scattering vector is $Q = \frac{4\pi \sin(\theta/2)}{\lambda}$, where λ is the wavelength of the incoming beam of neutrons and θ is the scattering angle (wavelength = 0.6 nm, 12 % spread).

The scattering intensity $I(Q)$ of non-interacting cylinders is given by the **equation**:

$$I(Q) = nV_p^2(\rho_p - \rho_s)^2 P(Q) \quad (3)$$

where n is the number density of scatterers, each having a volume V_p and scattering length density ρ_p ; ρ_s is the scattering length density of the solvent. $P(Q)$ is the form factor of a cylinder:

$$P_{\text{cyl}}(Q) = \langle A^2(Q) \rangle = \int_0^{\pi} A^2(Q, \alpha) \sin \alpha \, d\alpha \quad (4)$$

Here, $A(Q, \alpha)$ is the amplitude function of a cylinder, given by:

$$A(Q, \alpha) = \frac{\sin(QL \cos(\alpha)/2)}{QL \cos(\alpha)/2} \cdot \frac{2J_1(QR \sin(\alpha))}{QR \sin(\alpha)} \quad (5)$$

where $J_1(x)$ is the first-order Bessel function. Scattering data were reduced with NIST NCNR's IgorPro data reduction software and analyzed with Sasview⁸⁰.

Covalent Linking of Bundles

To form polymers of bundles, bundles were covalently linked *via* their N-termini as detailed previously.⁵⁶ A maleimide N-terminated variant of the **4B+4** peptide, Mal-**4B+4**, was created. An additional Cys was appended at the N-terminus of **4B+4** to yield the Cys-**4B+4** peptide. Lyophilized peptides were separately dissolved in distilled (DI) water to a concentration of **5 mM** to form each homomeric bundle. The two solutions were mixed in equimolar amounts, and 0.01 equivalent of tris(2- carboxyethyl)phosphine (TCEP, 50 mM in DI water) was added to prevent disulfide formation. The solution was shaken for 3 d at room temperature to produce rod-like

polymer chains. Similarly, the procedure was repeated with maleimide terminated **4B-4**, Mal-**4B-4**, and Cys-terminated **4B-4**, Cys-**4B-4**, to produce polymer chains.

Transmission Electron Microscopy

For TEM characterization, 200 mesh copper grids with coated carbon (CF200-Cu-UL) purchased from Electron Microscopy Sciences Inc were plasma treated (PDC-32G, Harrica Plasma Inc.) for 30 s. A 5 μL solution of bundle polymers in water (1 % weight/volume) was added to the carbon-side of the grid and allowed to sit for 1 min before blotting with a dry filter paper. Next, the sample was immediately **negatively** stained with 5 μL of freshly prepared 1 % sodium phosphotungstate (Sigma, pH 7.0) and blotted after 1 min to remove excess stain solution. The grid was dried for 1 h under air and used for TEM analysis. Cast-film TEM was performed on Thermo Scientific Talos F200C transmission electron microscope using 200 kV accelerating voltage equipped with a 4k x 4k CMOS camera Ceta 16M.

Results and Discussion

Computational Design of Tetrahelical Bundle Sequences

A *de novo* designed homotetrahelical bundle structure was selected that comprises four anti-parallel helices.⁵⁹ The bundle possesses a motif with D₂ symmetry, a hydrophobic interior core, and complementary methionine interactions. In previous studies, this bundle motif has supported substantial variation among its exterior residues.^{54, 59, 79} A series of residue substitutions were identified among the 18 exterior residues so as to span a range of putative charge states from $q = -8$ to $q = +8$. The calculations identified substitutions to ionizable residues (D, E, K, and R) so as to achieve a targeted putative charge q .

The peptide backbone used in the design computation was the previously reported tetrahelical backbone of BNDL1.⁵⁹ Each helical peptide in the homotetramer contains 29 residues. The 11 interior residues (sites 4, 7, 8, 11, 14, 15, 18, 21, 22, 25, 29, rendered in **Fig. 1a**) were previously designed so as to form a hydrophobic core, and the resulting tetramer has tolerated amino acid variation at exterior sites.^{54, 59, 79} To facilitate concentration measurements, an initial design calculation was run, allowing Tyr and the original BNDL1 amino acid at each of the 18 exterior sites. Residue 26 exhibited the largest Tyr probability, and Tyr26 was retained in the remaining calculations.

Starting from this Tyr26 variant of BNDL1 (DEEIRRMAEEIRQMAERIQQMAEQIYQEA, sequence ID **4B-3** in **Table 1**), amino acid substitutions were made stepwise to modify the putative charge q . Each step resulted in a sequence with a new net charge, eventually spanning $q = -8$ to $q = +8$ (**Table 1**). The putative charge q is a sum of charges over the N-terminal ammonium (+1) and Arg (+1), Lys (+1), Asp (-1) Glu (-1) side chains; all remaining residues and the C-terminal amide have charge states of 0. The backbone and the 11 interior residues were kept the same as

BNDL1. For exterior residues, site 26 was kept as Tyr, and the remaining 17 exterior residues (sites 1, 2, 3, 5, 6, 9, 10, 12, 13, 16, 17, 19, 20, 23, 24, 27, 28) were allowed to vary among 18 natural amino acids; Pro and Cys were excluded. Each new sequence was established by substituting one exterior amino acid residue within a previously identified (parent) sequence, and the resulting sequence had a new charge state (target charge) that differed by ± 1 or ± 2 . The net charge was constrained to the target charge during the calculation. For each variable site, we compared the probability of the most likely amino acid with that of the amino acid of the parent sequence using a quantitative measure of ‘mutability’ for a site: $r = \ln (w_{i,mp} / w_{i,ref})$, where $w_{i,mp}$ is the probability at site i of the most probable amino acid and $w_{i,ref}$ is the probability of the amino acid in the parent sequence (reference type).^{81, 82} Calculations proceeded in an iterative manner, where after each round of calculation, sites with $r = 0$ were constrained to be the amino acid in the parent sequence. Iterations were stopped when no sites with $r = 0$ were obtained, and the remaining sites were ranked by their r values. The substitution with the highest r value that yielded the targeted charge state was selected. The resulting sequence was then used as the parent in a subsequent calculation (see also supplementary information). The resulting peptides are listed in **Table 1**, where the sequences are labeled by their putative charges, e.g. **4B-8** refers to the tetramer-forming peptide with $q = -8$. Each homotetrameric bundle has a putative charge of $4q$. The putative net charge q neglects variation of side-chain pKa with location in the structure; herein we use q primarily to distinguish the sequences in terms of their presentation of ionizable residues. We note that **4B0** and experimental studies of its colloid-like behavior have been reported previously.⁵⁴

| ID | q | Sequence | T_m °C |
|-------------|----|--|----------|
| 4B-8 | -8 | DEEI ^{red} Q ^{grey} RM AEEI ^{red} R ^{grey} QM AEEI ^{red} D ^{grey} QM AEEI ^{red} Y ^{grey} Q ^{red} E A | 37 |
| 4B-7 | -7 | DEEI ^{red} Q ^{grey} RM AEEI ^{red} R ^{grey} QM AEEI ^{red} D ^{grey} QM AEQ ^{red} I ^{grey} Y ^{grey} Q ^{red} E A | 49 |
| 4B-6 | -6 | DEEI ^{red} Q ^{grey} RM AEEI ^{red} R ^{grey} QM AERI ^{red} D ^{grey} QM AEEI ^{red} Y ^{grey} Q ^{red} E A | 41 |
| 4B-5 | -5 | DEEI ^{red} Q ^{grey} RM AEEI ^{red} R ^{grey} QM AERI ^{red} D ^{grey} QM AEQ ^{red} I ^{grey} Y ^{grey} Q ^{red} E A | 56 |
| 4B-4 | -4 | DEEI ^{red} RR ^{grey} M AEEI ^{red} R ^{grey} QM AERI ^{red} D ^{grey} QM AEQ ^{red} I ^{grey} Y ^{grey} Q ^{red} E A | 52 |
| 4B-3 | -3 | DEEI ^{red} RR ^{grey} M AEEI ^{red} R ^{grey} QM AERI ^{red} QQ ^{grey} M AEQ ^{red} I ^{grey} Y ^{grey} Q ^{red} E A | - |
| 4B-2 | -2 | DEEI ^{red} RR ^{grey} M AEEI ^{red} R ^{grey} K ^{grey} M AERI ^{red} QQ ^{grey} M AEQ ^{red} I ^{grey} Y ^{grey} Q ^{red} E A | - |
| 4B-1 | -1 | DEEI ^{red} RR ^{grey} M AEEI ^{red} R ^{grey} K ^{grey} M AERI ^{red} K ^{grey} QM AEQ ^{red} I ^{grey} Y ^{grey} Q ^{red} E A | - |
| 4B0 | 0 | DEEI ^{red} RR ^{grey} M AEEI ^{red} R ^{grey} K ^{grey} M AERI ^{red} K ^{grey} QM AEQ ^{red} I ^{grey} Y ^{grey} K ^{red} E A | - |
| 4B+1 | +1 | DEEI ^{red} RR ^{grey} M AEEI ^{red} R ^{grey} K ^{grey} M AERI ^{red} KK ^{grey} M AEQ ^{red} I ^{grey} Y ^{grey} K ^{red} E A | - |
| 4B+2 | +2 | DKEI ^{red} RR ^{grey} M AEEI ^{red} R ^{grey} K ^{grey} M AERI ^{red} K ^{grey} QM AEQ ^{red} I ^{grey} Y ^{grey} K ^{red} E A | - |
| 4B+3 | +3 | DKEI ^{red} RR ^{grey} M AEEI ^{red} R ^{grey} K ^{grey} M AERI ^{red} KK ^{grey} M AEQ ^{red} I ^{grey} Y ^{grey} K ^{red} E A | - |
| 4B+4 | +4 | DKEI ^{red} RR ^{grey} M AEK ^{red} I ^{grey} R ^{grey} K ^{grey} M AERI ^{red} K ^{grey} QM AEQ ^{red} I ^{grey} Y ^{grey} K ^{red} E A | - |
| 4B+5 | +5 | DKEI ^{red} RR ^{grey} M AEK ^{red} I ^{grey} R ^{grey} K ^{grey} M AERI ^{red} KK ^{grey} M AEQ ^{red} I ^{grey} Y ^{grey} K ^{red} E A | - |
| 4B+6 | +6 | DKEI ^{red} RR ^{grey} M AEK ^{red} I ^{grey} R ^{grey} K ^{grey} M AERI ^{red} KK ^{grey} M AEK ^{red} I ^{grey} Y ^{grey} K ^{red} E A | - |
| 4B+7 | +7 | DKVI ^{red} RR ^{grey} M AKK ^{red} I ^{grey} R ^{grey} K ^{grey} M AERI ^{red} K ^{grey} QM AEQ ^{red} I ^{grey} Y ^{grey} K ^{red} E A | - |
| 4B+8 | +8 | DKEI ^{red} RR ^{grey} M AEK ^{red} I ^{grey} R ^{grey} K ^{grey} M AERI ^{red} KK ^{grey} M AEK ^{red} I ^{grey} Y ^{grey} K ^{red} R A | - |

Table 1. Designed sequences of tetrahelical bundles with net charges ranging from $q = -8$ to $q = +8$. Putative charge state q includes positively charged amino terminus and neutral C-terminal amide. The amino acids are colored by residue type: hydrophobic (grey), polar-nonionizable (black), positive (blue), and negative (red). T_m values were obtained from fitting the temperature dependence of the molar ellipticities per residue at 222 nm. If T_m is not reported, cooperative unfolding was not observed over the temperature range of $T = 10$ °C to $T = 80$ °C.

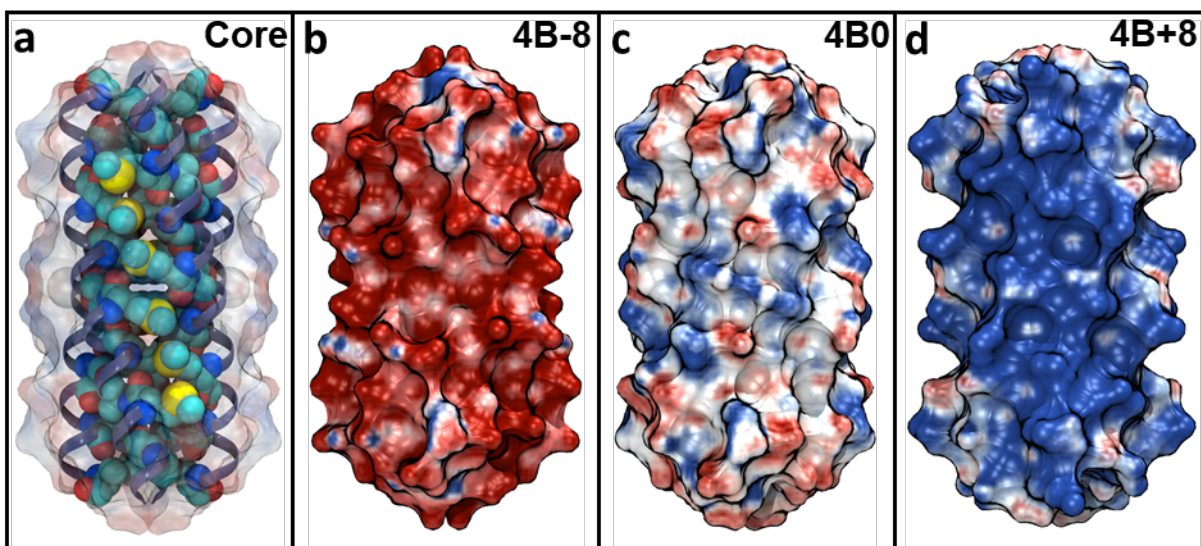


Figure 1. Renderings of model D_2 symmetric homotetrameric helical bundles. **(a)** Conserved residues and core structure of bundle. Conserved hydrophobic residues rendered as space filling. Electrostatic potential surface of **4B0** structure rendered as transparent. Mutations were made to remaining exterior residues to achieve putative charge states. **(b-d)** Electrostatic surface potential renderings of bundles comprising peptides **4B-8** **(b)**, **4B0** **(c)** and **4B+8** **(d)**. Electrostatic surfaces are colored red (negative) to blue (positive) using data obtained using APBS (Adaptive Poisson-Boltzmann Solver) tool⁸³ and rendered using VMD.⁷⁶

Circular Dichroic Spectroscopy

Circular dichroic (CD) spectra of the designed peptides were consistent with alpha helical, coiled-coil structure formation. Distinct minima in the ellipticity appeared at 208 nm and 222 nm. In the temperature-dependent studies, the molar ellipticity per residue at 222 nm was monitored as an indicator of helical structure. For each sequence where cooperative unfolding was observed, fitting the temperature-dependent data using an oligomeric, two-state model⁸⁴ (see SI) yielded the

melting temperature T_m . The negatively charged sequences corresponding to $q = -4, -5, -6, -7, -8$ had T_m values over the range of $T_m = 37$ °C to $T_m = 56$ °C (**Table 1**), whereas no such transition was observed for sequences with $q = -3$ to $+8$ (thermal curves are included in SI). The high thermal stability, particularly for positively charged sequences, highlights the robustness of the *de novo* designed structure with respect to exterior variation. Interestingly, a single substitution Q19D (mutating residue 19 from Q to D) in peptide **4B-3** caused a transition from $T_m > 80$ °C for **4B-3** to $T_m = 52$ °C for **4B-4**.

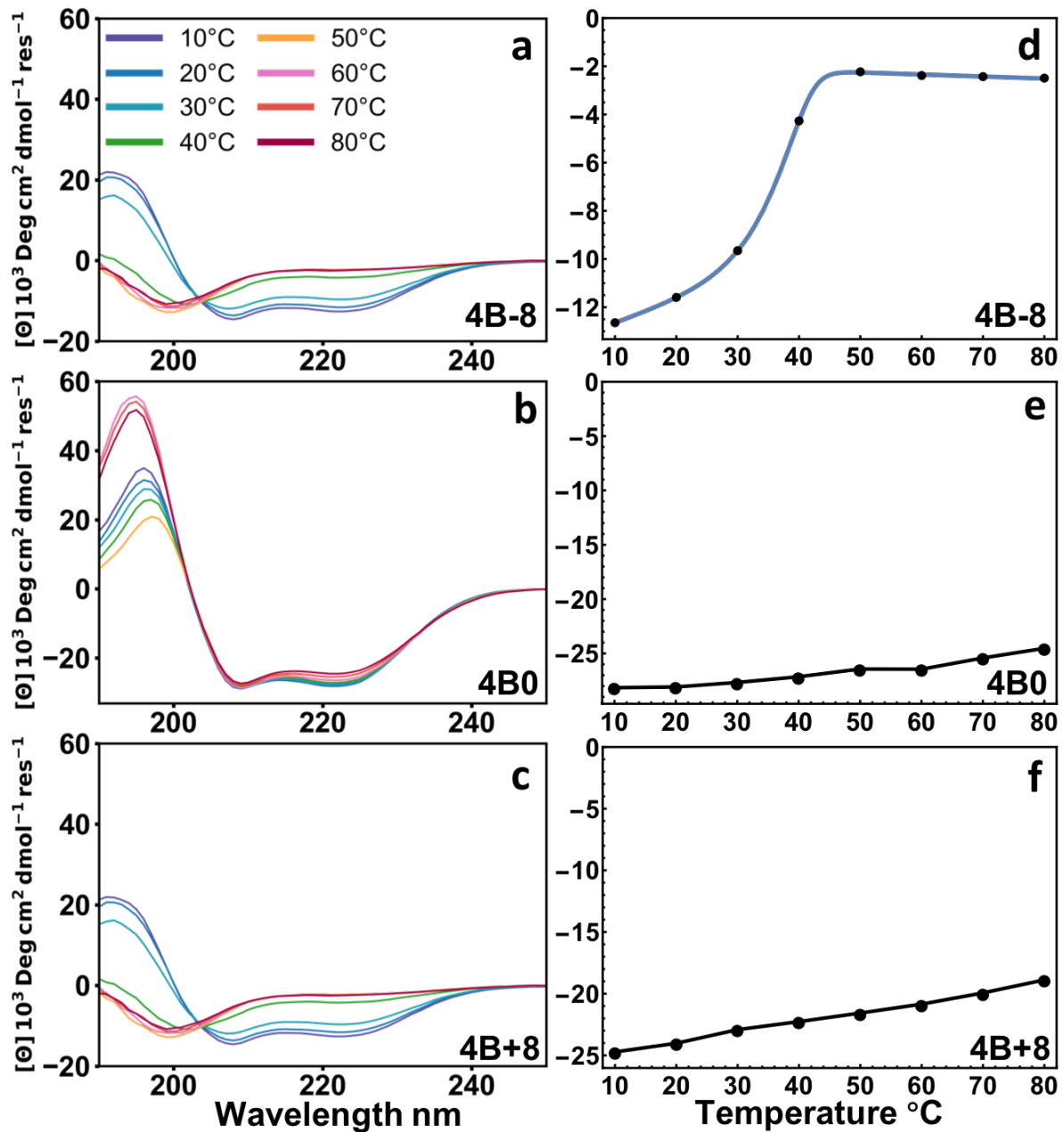


Figure 2. Circular dichroic (CD) spectra for pH 7 and 100 μM peptide. (a-c) CD spectra of peptides (a) *4B-8*, (b) *4B0*⁵⁴ and (c) *4B+8* at various temperatures. All three panels (a-c) share the same coloring scheme shown in a. (d-f) Mean residue ellipticities at 222nm of (d) *4B-8*, (e) *4B0*, and

(f) $4B+8$ versus temperature. Data in (d) are fit to two-state oligomerization model (blue curve). No cooperative unfolding observed for (e) $4B0$ and (f) $4B+8$.

Analytical Ultracentrifugation.

Sedimentation velocity analytical ultracentrifugation (AUC) measurements were conducted to measure the molecular weight of the predominant oligomeric species in solution for a subset of the designed peptides. For each sequence, the molecular weight corresponding to the major sedimenting peak was calculated using Eq. 2, and the data are summarized in Fig. 3 (see SI for individual AUC data and fits). The oligomerization state of the sedimenting species for each peptide is consistent with the formation of the homotetramer.

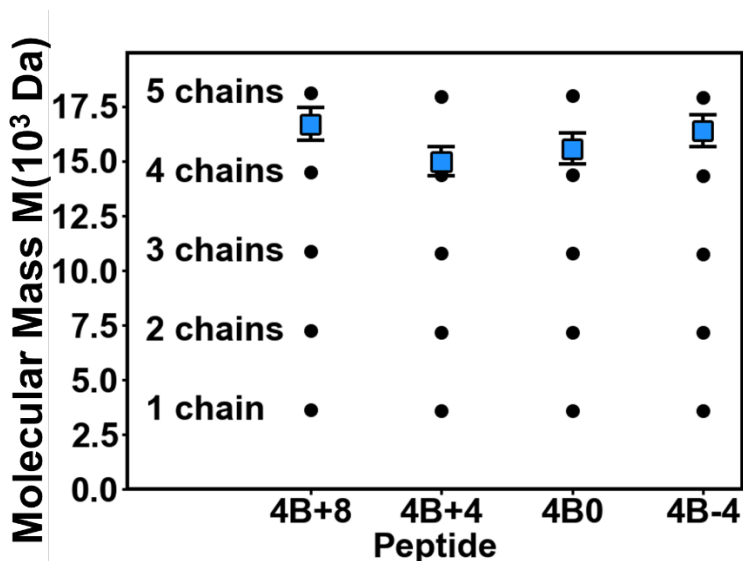


Figure 3. Analytical ultracentrifugation (AUC) data. Molecular mass (M) determination of computationally designed bundles using AUC. The measured M (blue squares) of the major sedimenting species is compared with the expected M (black circles) for a homo-oligomer states

(1-5 chains) of the computationally designed peptides. An uncertainty of $\bar{v} \pm 1\%$ leads to an estimated uncertainty of $\pm 4.5\%$ in molecular mass, which is indicated as error bars.

Small Angle Neutron Scattering

To characterize the bundle shape in solution, small angle neutron scattering (SANS) measurements were performed on dilute solutions (0.25 mass %) of a subset of the designed sequences: *4B-6*, *4B-4*, *4B0*, *4B+4* and *4B+8* (see Fig. 4, Fig. S42 and Table S2). The data for each peptide can be described by a cylinder form factor, and the fit to SANS data for peptide *4B0* is shown in Fig. 4 (see Fig. S42 and Table S2 for all fits). The fitted parameters reveal that the bundles have the same cylindrical shape; the extracted radii (1.04 – 1.15 nm) and cylinder lengths ((3.7 – 4.5) nm) are consistent with the targeted model structure and are in close agreement with previous results for BNDL1.^{59, 79}

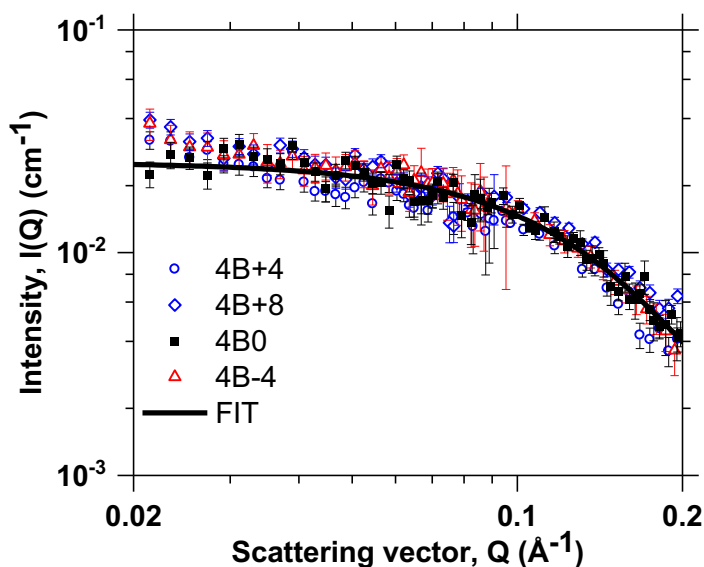


Figure 4. Small angle neutron scattering (SANS) data. SANS scattering intensity $I(Q)$ of bundle samples containing 0.25 mass % peptide in deuterium oxide (D_2O). Cylinder form factor fit to

SANS data for **4B0** data is plotted as a solid black line. Error bars on data points indicate \pm one standard deviation.

Molecular Dynamics Simulations of Designed Peptide Bundles

MD simulations were performed on all designed peptides to study their structural fluctuations. Each peptide bundle maintained the tetrahelical folded structure throughout the corresponding 40 ns simulation. The overall trend observed was that the N- and C-termini had higher structural fluctuations than the central region of the bundle. The fluctuation of each residue with respect to the designed structure was characterized by the root-mean-square deviation (RMSD) of the residue's backbone atoms sampled every 20 ps during the second half of the simulation (20 to 40 ns). Data for **4B-8**, **4B0** and **4B+8** peptides appear in **Fig. 5(b-d)**. The structure of residues 7 to 22 was well conserved with backbone RMSD values of \approx 0.1 nm or lower. **At the ends of the bundle, the N-terminal residues showed larger structural fluctuations than those near the C-termini. N terminal residues were observed to uncoil and fray from the helical structure (Fig. 5a).**

We note that residue 19Q in **4B-3** was substituted to D in **4B-4**, which resulted in a decrease in the melting temperature from $T_m > 80$ °C for **4B-3** to $T_m = 52$ °C for **4B-4**. **While estimates of thermal stability are outside the scope of these simulations, the reduction in T_m may potentially be associated with introducing additional repulsive electrostatic interactions between negatively charged residues in a well-structured helical region. The Q19D substitution sandwiches D19 between E16 and E23. The resulting intrahelical electrostatic interactions involving the three negatively charged residues may destabilize the bundle and yield the reduced T_m observed for **4B-4**.**

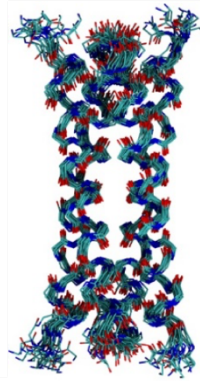
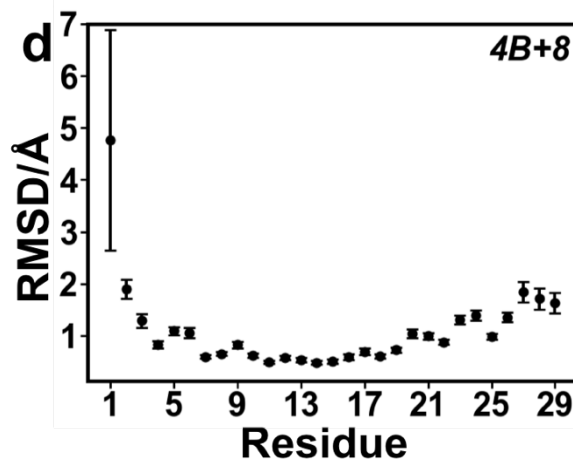
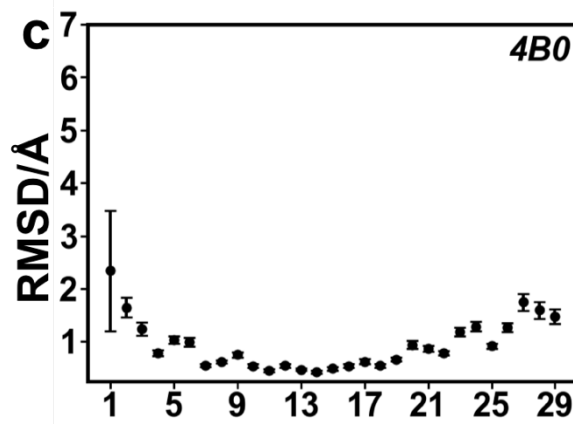
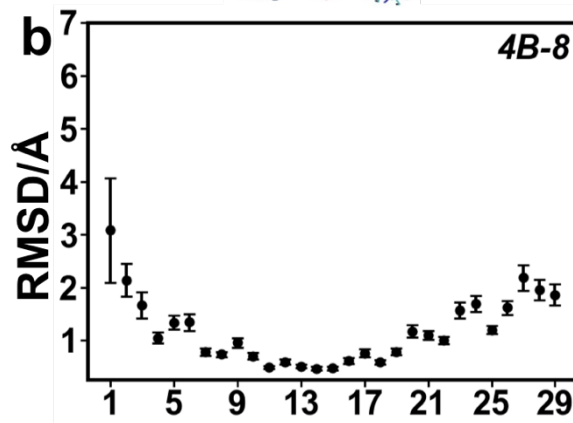
a**4B-8**

Figure 5. Molecular dynamics (MD) simulations. **(a)** Superposition of 20 backbone structures from MD simulation of **4B-8** (sampled every 2ns over 40 ns). **(b-d)** RMSD relative to model structure of backbone atoms for each residue in simulated structures of **4B-8** **(b)**, **4B0** **(c)** and **4B+8** **(d)**. Average values (plotted as dots) and standard deviations (error bars are +/- one standard deviation) of the RMSD calculated using 2000 sampled structures and include equivalent positions at each of the four helices.

Redesigned Sequences 4B-6 and 4B-8

Of the 17 sequences originally designed for the targeted charge states spanning $q = -8$ to $+8$, 15 were observed experimentally to fold as intended. However, the original sequences for $q = -6$ and $q = -8$ (labeled in **Table 2** as **4B-6orig** and **4B-8orig**) did not form helical secondary structures, as indicated by their CD spectra (**Fig. S22** and **S25**). Relative to **4B-5**, the **4B-6orig** sequence contained a Q5E substitution, and the **4B-8orig** sequence contained both the Q5E and R17E substitutions. The Q5E substitution was suspected to be associated with the decreased helical structure. Noting that these sequences each contain DEE at the N-terminus, replacing residue Q5 with E may destabilize the structure due to further crowding the N-terminal region with negative charge. Consequently, the redesign calculations did not allow E or D at residues 5 and 6. The resulting computational design yielded the **4B-6** and **4B-8** sequences (**Table 1** and **2**). The redesigned peptides displayed helical features in their CD spectra (**Fig. S23** and **S26**). This refinement of problematic sequences demonstrates how combined computational and experimental approaches can yield principles for design of these bundles.

| ID | Sequence |
|-----------------|-----------------------------------|
| 4B-6orig | DEEIERM AEEIRQM AERIDQM AEQIYQE A |
| 4B-8orig | DEEIERM AEEIRQM AEEIDQM AEQIYQE A |
| 4B-6 | DEEIQRM AEEIRQM AERIDQM AEEIYQE A |
| 4B-8 | DEEIQRM AEEIRQM AEEIDQM AEEIYQE A |

Table 2. Redesigned sequences for $q = -6$ and $q = -8$. Original sequences: **4B-6orig** and **4B-8orig**.

Sequences **4B-6** and **4B-8** also appear in **Table 1**.

Transmission Electron Microscopy of Covalently Linked Peptide Bundles

In previous studies, related 29-residue D_2 symmetric homotetrameric bundles were covalently linked via functionalization of their N termini to yield rigid polymers.⁵⁵⁻⁵⁷ Charged bundles designed herein can be similarly polymerized. The polymer comprises two types of bundle monomers (bundlemers⁵⁵⁻⁵⁷), each having different functionalization at the N terminus of the peptide: (a) a bundle with maleimide (Mal) attached via the amino terminus, and (b) a 30-residue bundle with an additional Cys residue at the N terminus (**Fig. 6a**). Given the anti-parallel D_2 symmetry, each end of the corresponding bundle monomer displays (a) two maleimide groups or (b) two thiol groups. Covalent bonds form between maleimides and the Cys thiols, resulting in doubly linked monomers and an alternating Mal-bundle/Cys-bundle copolymer (**Fig. 6a**). Two polymers were synthesized, one consisting of only **4B+4** and the other consisting of only **4B-4**. The resulting structures were characterized by transmission electron microscopy (TEM). Each exhibited rigid-rod-like behavior (**Fig. 6**). The positively charged polymers constructed using **4B+4** tended to associate and align in a parallel fashion, forming straight tubular structures (**Fig. 6b**). The negatively charged **4B-4** polymers were less association prone (**Fig. 6c**). The phosphotungstate anions of the stain solution may have mediated aggregation of the positively charged **4B+4** polymers, consistent with previously observed ion-mediated aggregation of bundles

in solution.⁵⁴ Conversely, phosphotungstate appeared to facilitate dispersion of the negatively charged *4B-4* polymers.

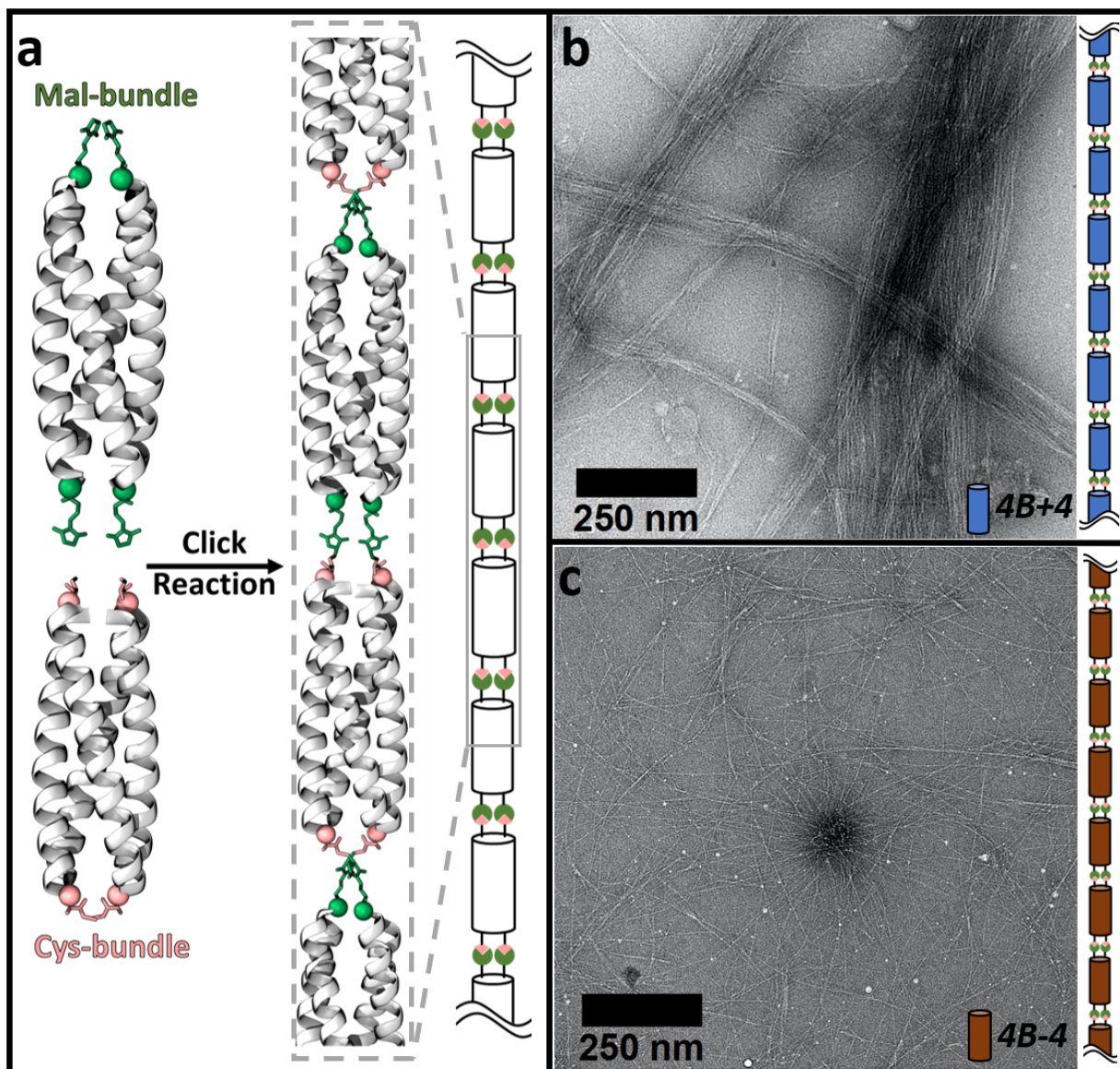


Figure 6. Polymers of functioned bundles. (a) Bundles linked by thiol-maleimide linkages. (b-c) Transmission electron micrographs (TEM) of cast-film and negatively stained polymeric assemblies of *4B+4* (b) and *4B-4* (c).

Conclusion

A set of seventeen 29-residue peptides that span putative charge states from $q = -8$ to $q = +8$ have been computationally designed to form a common homotetrameric helical bundle structure; the putative charges of the bundles thus vary over the range $q = -32$ to $q = +32$. Taken together, the experimental results provide complementary evidence that the peptides form the targeted bundle structure in solution. CD spectroscopy confirmed the helical secondary structure at pH 7. The AUC studies yielded molecular weights consistent with the homotetrameric state. The SANS studies were well fit by a cylindrical model with the expected dimensions of the peptide bundles. The majority (12) of the sequences were highly thermostable, possessing melting temperatures of $T_m > 80$ °C. Temperature-dependent studies of five of the most negatively charged sequences, each having a cluster of negatively charged residues at the N terminus, were well-fit by a two-state oligomerization model; these sequences exhibited melting temperatures T_m from 37 to 56 °C. The melting temperature of a bundle thus is sensitive to the sequence positioning of ionizable residues, suggesting routes to modulating the stabilities of the bundles. The bundles were polymerized via complementary chemical functionalization of the N-termini of their constituent peptides, yielding polymers with rigid-rod-like structures.⁵⁶ The resulting peptides provide a route to a suite of tetrameric bundles, where the number of ionizable groups and putative charge can be varied incrementally without changing the structure. These bundles provide well-structured proteins for studies of protein-protein interactions, protein electrostatic effects, colloidal properties, and polyelectrolytes with controlled charge and stiffness.

Associated Content

The supporting information is available free of charge. Illustration of the D_2 symmetry and hydrophobic core of the homotetrameric helical bundle. Surface rendering of the tetrahelical bundles with different putative charges. Experimental results: UPLC and mass spectrograms of the peptide bundles. CD spectra and melting curves of the peptide bundles. AUC data and fit results for a subset of the peptides. SANS data and fit results for a subset of the peptides.

Author Information

Corresponding Author

Darrin J. Pochan - Department of Materials Science and Engineering, University of Delaware, Newark, Delaware 19716, United States. Email: pochan@udel.edu

Jeffery G. Saven - Department of Chemistry, University of Pennsylvania, Philadelphia, Pennsylvania 19104, United States. Email: saven@upenn.edu

Author Contributions

Rui Guo performed the computational design, MD simulations and redesign of the peptides. Nairiti J. Sinha performed AUC with Jeffery A. Fagan and SANS characterization with Grethe Jensen. Rajkumar Misra synthesized and purified the peptides and collected UPLC, mass spectrograms and CD experimental data. Yao Tang and Matthew Langenstein covalently linked the peptide bundles and obtained the TEM images of the linked bundles with Kyunghee Kim. Jeffery G. Saven, Christopher J. Kloxin and Darrin J. Pochan oversaw the project and provided guidance. All authors have given approval to the final version of the manuscript.

Acknowledgement and Funding Sources

Support for peptide design, synthesis, purification, and bundle rod formation was provided by the Department of Energy, Office of Basic Energy Sciences, Biomolecular Materials Program under grant No. DE-SC0019355 and DE-SC0019282. The manuscript preparation also was supported by cooperative agreement #370NANB17H302 from National Institute of Standards and Technology (NIST), U.S. Department of Commerce. We acknowledge the support of the NIST, U.S. Department of Commerce in providing the neutron research facilities used in this work. Access to vSANS and NSE was provided by the Center for High Resolution Neutron Scattering (CHRNS), a partnership between the National Institute of Standards and Technology and the National Science Foundation under Agreement No. DMR-1508249. Samples were prepared for experiments at the NIST/IBBR Biomolecular Labeling Laboratory. **The authors acknowledge the use of facilities and instrumentation supported by NSF through the University of Delaware Materials Research Science and Engineering Center, DMR-2011824.** This work used the Extreme Science and Engineering Discovery Environment (XSEDE)⁸⁵, which is supported by National Science Foundation grant number ACI-1548562; XSEDE *stampede2* resources were utilized through allocation *TG-CHE110041*. This work benefited from the use of the SasView application, originally developed under NSF award DMR-0520547. SasView contains code developed with funding from the European Union's Horizon 2020 research and innovation programme under the SINE2020 project, grant agreement No 654000. We thank Dr. Yun Liu and Dr. Paul Butler for their insights and comments.

Disclaimer

The statements, findings, conclusions, and recommendations are those of the authors and do not necessarily reflect the view of NIST or the U.S. Department of Commerce. Certain commercial

equipment, instruments, materials, suppliers, and software are identified in this paper to foster understanding. Such identification does not imply recommendation or endorsement by the NIST, nor does it imply that the materials or equipment identified are necessarily the best available for the purpose.

Abbreviations

CD, Circular Dichroism; AUC, analytical ultracentrifugation; SANS, small angle neutron scattering; TEM, transmission electron microscopy; MD, molecular dynamics; VMD, Visual Molecular Dynamics; NAMD, Nanoscale Molecular Dynamics; DMF, N, N-dimethylformamide; TFA, trifluoroacetic acid; TIPS, triisopropylsilane; DIC, diisopropylcarbodiimide; Oxyma, ethyl (hydroxyimino)cyanoacetate; HPLC, high pressure liquid chromatography

References

1. Leader, B.; Baca, Q. J.; Golan, D. E., Protein therapeutics: A summary and pharmacological classification. *Nat. Rev. Drug Discovery* **2008**, *7* (1), 21-39.
2. Dimitrov, D. S., Therapeutic proteins. *Methods Mol. Biol.* **2012**, *899*, 1-26.
3. DeFrates, K. G.; Moore, R.; Borgesi, J.; Lin, G. W.; Mulderig, T.; Beachley, V.; Hu, X., Protein-Based Fiber Materials in Medicine: A Review. *J. Nanomater.* **2018**, *8* (7), 457.
4. Reddy, N.; Yang, Y. Q., Potential of plant proteins for medical applications. *Trends Biotechnol.* **2011**, *29* (10), 490-498.

5. Hong, S.; Choi, D. W.; Kim, H. N.; Park, C. G.; Lee, W.; Park, H. H., Protein-Based Nanoparticles as Drug Delivery Systems. *Pharmaceutics* **2020**, *12* (7), 604.
6. Hamley, I. W., Small Bioactive Peptides for Biomaterials Design and Therapeutics. *Chem. Rev.* **2017**, *117* (24), 14015-14041.
7. Chu, S.; Wang, A. L.; Bhattacharya, A.; Montclare, J. K., Protein based biomaterials for therapeutic and diagnostic applications. *Prog. Biomed. Eng.* **2021**, *4* (1), 012003.
8. Damodaran, S., Food Proteins: An Overview. In *Food Proteins and Their Applications*, Marcel Dekker: New York, NY, USA, 1997; pp 1-25.
9. Chen, L. Y.; Remondetto, G. E.; Subirade, M., Food protein-based materials as nutraceutical delivery systems. *Trends Food Sci. Technol.* **2006**, *17* (5), 272-283.
10. Tomadoni, B.; Capello, C.; Valencia, G. A.; Gutierrez, T. J., Self-assembled proteins for food applications: A review. *Trends Food Sci. Technol.* **2020**, *101*, 1-16.
11. Benkovic, S. J.; Hammes-Schiffer, S., A perspective on enzyme catalysis. *Science* **2003**, *301* (5637), 1196-1202.
12. Warshel, A.; Sharma, P. K.; Kato, M.; Xiang, Y.; Liu, H. B.; Olsson, M. H. M., Electrostatic basis for enzyme catalysis. *Chem. Rev.* **2006**, *106* (8), 3210-3235.
13. Hammes, G. G.; Benkovic, S. J.; Hammes-Schiffer, S., Flexibility, Diversity, and Cooperativity: Pillars of Enzyme Catalysis. *Biochemistry* **2011**, *50* (48), 10422-10430.
14. Intasian, P.; Prakinee, K.; Phintha, A.; Trisrivirat, D.; Weeranoppanant, N.; Wongnate, T.; Chaiyen, P., Enzymes, In Vivo Biocatalysis, and Metabolic Engineering for Enabling a Circular Economy and Sustainability. *Chem. Rev.* **2021**, *121* (17), 10367-10451.
15. Chen, K.; Arnold, F. H., Engineering new catalytic activities in enzymes. *Nat. Catal.* **2020**, *3* (3), 203-213.

16. Goldsmith, M.; Tawfik, D. S., Enzyme engineering: reaching the maximal catalytic efficiency peak. *Curr. Opin. Struct. Biol.* **2017**, *47*, 140-150.
17. de la Rica, R.; Matsui, H., Applications of peptide and protein-based materials in bionanotechnology. *Chem. Soc. Rev.* **2010**, *39* (9), 3499-3509.
18. Hamley, I. W., Protein Assemblies: Nature-Inspired and Designed Nanostructures. *Biomacromolecules* **2019**, *20* (5), 1829-1848.
19. Whyburn, G. P.; Li, Y. J.; Huang, Y., Protein and protein assembly based material structures. *J. Mater. Chem.* **2008**, *18* (32), 3755-3762.
20. DeFrates, K.; Markiewicz, T.; Gallo, P.; Rack, A.; Weyhmiller, A.; Jarmusik, B.; Hu, X., Protein Polymer-Based Nanoparticles: Fabrication and Medical Applications. *Int. J. Mol. Sci.* **2018**, *19* (6), 1717.
21. Sinha, N. J.; Langenstein, M. G.; Pochan, D. J.; Kloxin, C. J.; Saven, J. G., Peptide Design and Self-assembly into Targeted Nanostructure and Functional Materials. *Chem. Rev.* **2021**, *121* (22), 13915–13935.
22. Conticello, V.; Hughes, S.; Modlin, C., Biomaterials Made from Coiled-Coil Peptides. In *Fibrous Proteins: Structures and Mechanisms*, Parry, D. A. D.; Squire, J. M., Eds. Springer International Publishing: Cham, 2017; pp 575-600.
23. Wei, G.; Su, Z. Q.; Reynolds, N. P.; Arosio, P.; Hamley, I. W.; Gazit, E.; Mezzenga, R., Self-assembling peptide and protein amyloids: from structure to tailored function in nanotechnology. *Chem. Soc. Rev.* **2017**, *46* (15), 4661-4708.
24. Lin, C. Y.; Liu, J. C., Modular protein domains: an engineering approach toward functional biomaterials. *Curr. Opin. Biotechnol.* **2016**, *40*, 56-63.

25. Katyal, P.; Meleties, M.; Montclare, J. K., Self-Assembled Protein- and Peptide-Based Nanomaterials. *ACS Biomater. Sci. Eng.* **2019**, *5* (9), 4132-4147.
26. Hamley, I. W., Peptide fibrillization. *Angew. Chem., Int. Ed.* **2007**, *46* (43), 8128-8147.
27. Hamley, I. W., Peptide Nanotubes. *Angew. Chem., Int. Ed.* **2014**, *53* (27), 6866-6881.
28. Hume, J.; Sun, J.; Jacquet, R.; Renfrew, P. D.; Martin, J. A.; Bonneau, R.; Gilchrist, M. L.; Montclare, J. K., Engineered Coiled-Coil Protein Microfibers. *Biomacromolecules* **2014**, *15* (10), 3503-3510.
29. Ling, S. J.; Kaplan, D. L.; Buehler, M. J., Nanofibrils in nature and materials engineering. *Nat. Rev. Mater.* **2018**, *3* (4), 18016.
30. Thomas, F.; Burgess, N. C.; Thomson, A. R.; Woolfson, D. N., Controlling the Assembly of Coiled-Coil Peptide Nanotubes. *Angew. Chem., Int. Ed.* **2016**, *55* (3), 987-991.
31. Burgess, N. C.; Sharp, T. H.; Thomas, F.; Wood, C. W.; Thomson, A. R.; Zaccai, N. R.; Brady, R. L.; Serpell, L. C.; Woolfson, D. N., Modular Design of Self-Assembling Peptide-Based Nanotubes. *J. Am. Chem. Soc.* **2015**, *137* (33), 10554-10562.
32. Xu, C. F.; Liu, R.; Mehta, A. K.; Guerrero-Ferreira, R. C.; Wright, E. R.; Dunin-Horkawicz, S.; Morris, K.; Serpell, L. C.; Zuo, X. B.; Wall, J. S.; Conticello, V. P., Rational Design of Helical Nanotubes from Self-Assembly of Coiled-Coil Lock Washers. *J. Am. Chem. Soc.* **2013**, *135* (41), 15565-15578.
33. Merg, A. D.; Touponse, G.; van Genderen, E.; Zuo, X. B.; Bazrafshan, A.; Blum, T.; Hughes, S.; Salaita, K.; Abrahams, J. P.; Conticello, V. P., 2D Crystal Engineering of Nanosheets Assembled from Helical Peptide Building Blocks. *Angew. Chem., Int. Ed.* **2019**, *58* (38), 13507-13512.

34. Merg, A. D.; Touponse, G.; van Genderen, E.; Blum, T. B.; Zuo, X. B.; Bazrafshan, A.; Siaw, H. M. H.; McCanna, A.; Dyer, R. B.; Salaita, K.; Abrahams, J. P.; Conticello, V. P., Shape-Shifting Peptide Nanomaterials: Surface Asymmetry Enables pH-Dependent Formation and Interconversion of Collagen Tubes and Sheets. *J. Am. Chem. Soc.* **2020**, *142* (47), 19956-19968.
35. Wang, F.; Gnewou, O.; Modlin, C.; Beltran, L. C.; Xu, C.; Su, Z.; Juneja, P.; Grigoryan, G.; Egelman, E. H.; Conticello, V. P., Structural analysis of cross α -helical nanotubes provides insight into the designability of filamentous peptide nanomaterials. *Nat. Commun.* **2021**, *12* (1), 407.
36. Yang, Y. J.; Holmberg, A. L.; Olsen, B. D., Artificially Engineered Protein Polymers. In *Annu. Rev. Chem. Biomol. Eng.*, Prausnitz, J. M., Ed. 2017; Vol. 8, pp 549-575.
37. Chang, D.; Olsen, B. D., Self-assembly of protein-zwitterionic polymer bioconjugates into nanostructured materials. *Polym. Chem.* **2016**, *7* (13), 2410-2418.
38. Carbeck, J. D.; Colton, I. J.; Anderson, J. R.; Deutch, J. M.; Whitesides, G. M., Correlations between the charge of proteins and the number of ionizable groups they incorporate: Studies using protein charge ladders, capillary electrophoresis, and Debye-Huckel theory. *J. Am. Chem. Soc.* **1999**, *121* (46), 10671-10679.
39. Gitlin, I.; Carbeck, J. D.; Whitesides, G. M., Why are proteins charged? Networks of charge-charge interactions in proteins measured by charge ladders and capillary electrophoresis. *Angew. Chem., Int. Ed.* **2006**, *45* (19), 3022-3060.
40. Lawrence, M. S.; Phillips, K. J.; Liu, D. R., Supercharging proteins can impart unusual resilience. *J. Am. Chem. Soc.* **2007**, *129* (33), 10110-10112.

41. Thompson, D. B.; Cronican, J. J.; Liu, D. R., Engineering and Identifying Supercharged Proteins for Macromolecule Delivery Into Mammalian Cells. *Methods Enzymol.* **2012**, *503*, 293-319.
42. Ma, C.; Malessa, A.; Boersma, A. J.; Liu, K.; Herrmann, A., Supercharged Proteins and Polypeptides. *Adv. Mater.* **2020**, *32* (20), 1905309.
43. Miklos, A. E.; Kluwe, C.; Der, B. S.; Pai, S. P.; Sircar, A.; Hughes, R. A.; Berrondo, M.; Xu, J. Q.; Codrea, V.; Buckley, P. E.; Calm, A. M.; Welsh, H. S.; Warner, C. R.; Zacharko, M. A.; Carney, J. P.; Gray, J. J.; Georgiou, G.; Kuhlman, B.; Ellington, A. D., Structure-Based Design of Supercharged, Highly Thermoresistant Antibodies. *Chem. Biol.* **2012**, *19* (4), 449-455.
44. Johnson, L. B.; Park, S.; Gintner, L. P.; Snow, C. D., Characterization of supercharged cellulase activity and stability in ionic liquids. *J. Mol. Catal. B: Enzym.* **2016**, *132*, 84-90.
45. Haarmeyer, C. N.; Smith, M. D.; Chundawat, S. P. S.; Sammond, D.; Whitehead, T. A., Insights into cellulase-lignin non-specific binding revealed by computational redesign of the surface of green fluorescent protein. *Biotechnol. Bioeng.* **2017**, *114* (4), 740-750.
46. Whitehead, T. A.; Bandi, C. K.; Berger, M.; Park, J.; Chundawat, S. P. S., Negatively Supercharging Cellulases Render Them Lignin-Resistant. *ACS Sustainable Chem. Eng.* **2017**, *5* (7), 6247-6252.
47. Slovic, A. M.; Kono, H.; Lear, J. D.; Saven, J. G.; DeGrado, W. F., Computational design of water-soluble analogues of the potassium channel KcsA. *Proc. Natl. Acad. Sci. U. S. A.* **2004**, *101* (7), 1828-1833.
48. Slovic, A. M.; Summa, C. M.; Lear, J. D.; DeGrado, W. F., Computational design of a water-soluble analog of phospholamban. *Protein Sci.* **2003**, *12* (2), 337-348.

49. Perez-Aguilar, J. M.; Xi, J.; Matsunaga, F.; Cui, X.; Selling, B.; Saven, J. G.; Liu, R. Y., A Computationally Designed Water-Soluble Variant of a G-Protein-Coupled Receptor: The Human Mu Opioid Receptor. *Plos One* **2013**, *8* (6), e66009.
50. Hojgaard, C.; Kofoed, C.; Espersen, R.; Johansson, K. E.; Villa, M.; Willemoes, M.; Lindorff-Larsen, K.; Teilum, K.; Winther, J. R., A Soluble, Folded Protein without Charged Amino Acid Residues. *Biochemistry* **2016**, *55* (28), 3949-3956.
51. Hervo-Hansen, S.; Hojgaard, C.; Johansson, K. E.; Wang, Y.; Wahni, K.; Young, D.; Messens, J.; Teilum, K.; Lindorff-Larsen, K.; Winther, J. R., Charge Interactions in a Highly Charge-Depleted Protein. *J. Am. Chem. Soc.* **2021**, *143* (6), 2500-2508.
52. Biok, N. A.; Passow, A. D.; Wang, C. X.; Bingman, C. A.; Abbott, N. L.; Gellman, S. H., Retention of Coiled-Coil Dimer Formation in the Absence of Ion Pairing at Positions Flanking the Hydrophobic Core. *Biochemistry* **2019**, *58* (48), 4821-4826.
53. Simon, A. J.; Zhou, Y.; Ramasubramani, V.; Glaser, J.; Pothukuchy, A.; Gollihar, J.; Gerberich, J. C.; Leggere, J. C.; Morrow, B. R.; Jung, C.; Glotzer, S. C.; Taylor, D. W.; Ellington, A. D., Supercharging enables organized assembly of synthetic biomolecules. *Nat. Chem.* **2019**, *11* (3), 204-212.
54. Sinha, N. J.; Guo, R.; Misra, R.; Fagan, J.; Faraone, A.; Kloxin, C. J.; Saven, J. G.; Jensen, G. V.; Pochan, D. J., Colloid-like solution behavior of computationally designed coiled coil bundlers. *J. Colloid Interface Sci.* **2022**, *606*, 1974-1982.
55. Sinha, N. J.; Shi, Y.; Tang, Y.; Kloxin, C. J.; Saven, J. G.; Faraone, A.; Jensen, G. V.; Pochan, D. J., Intramolecular structure and dynamics in computationally designed peptide-based polymers displaying tunable chain stiffness. *Phys. Rev. Mater.* **2021**, *5* (9), 095601.

56. Wu, D. D.; Sinha, N.; Lee, J.; Sutherland, B. P.; Halaszynski, N. I.; Tian, Y.; Caplan, J.; Zhang, H. V.; Saven, J. G.; Kloxin, C. J.; Pochan, D. J., Polymers with controlled assembly and rigidity made with click-functional peptide bundles. *Nature* **2019**, *574* (7780), 658-662.
57. Sinha, N. J.; Wu, D. D.; Kloxin, C. J.; Saven, J. G.; Jensen, G. V.; Pochan, D. J., Polyelectrolyte character of rigid rod peptide bundlemer chains constructed via hierarchical self-assembly. *Soft Matter* **2019**, *15* (48), 9858-9870.
58. Diaz, J. E.; Lin, C. S.; Kunishiro, K.; Feld, B. K.; Avrantinis, S. K.; Bronson, J.; Greaves, J.; Saven, J. G.; Weiss, G. A., Computational design and selections for an engineered, thermostable terpene synthase. *Protein Sci.* **2011**, *20* (9), 1597-1606.
59. Zhang, H. V.; Polzer, F.; Haider, M. J.; Tian, Y.; Villegas, J. A.; Kiick, K. L.; Pochan, D. J.; Saven, J. G., Computationally designed peptides for self-assembly of nanostructured lattices. *Sci. Adv.* **2016**, *2* (9), 1600307.
60. DeGrado, W. F.; Summa, C. M.; Pavone, V.; Natri, F.; Lombardi, A., De novo design and structural characterization of proteins and metalloproteins. *Annu Rev Biochem* **1999**, *68*, 779-819.
61. Walsh, S. T.; Cheng, H.; Bryson, J. W.; Roder, H.; DeGrado, W. F., Solution structure and dynamics of a de novo designed three-helix bundle protein. *Proc Natl Acad Sci U S A* **1999**, *96* (10), 5486-91.
62. Derek, N. W., A Brief History of De Novo Protein Design: Minimal, Rational, and Computational. *J. Mol. Biol.* **2021**, *433*, 167160.
63. Thomas, F.; Boyle, A. L.; Burton, A. J.; Woolfson, D. N., A Set of de Novo Designed Parallel Heterodimeric Coiled Coils with Quantified Dissociation Constants in the Micromolar to Sub-nanomolar Regime. *J. Am. Chem. Soc.* **2013**, *135* (13), 5161-5166.

64. Huang, P. S.; Oberdorfer, G.; Xu, C. F.; Pei, X. Y.; Nannenga, B. L.; Rogers, J. M.; DiMaio, F.; Gonen, T.; Luisi, B.; Baker, D., High thermodynamic stability of parametrically designed helical bundles. *Science* **2014**, *346* (6208), 481-485.
65. McAllister, K. A.; Zou, H. L.; Cochran, F. V.; Bender, G. M.; Senes, A.; Fry, H. C.; Nanda, V.; Keenan, P. A.; Lear, J. D.; Saven, J. G.; Therien, M. J.; Blasie, J. K.; DeGrado, W. F., Using alpha-helical coiled-coils to design nanostructured metalloporphyrin arrays. *J. Am. Chem. Soc.* **2008**, *130* (36), 11921-11927.
66. Thomson, A. R.; Wood, C. W.; Burton, A. J.; Bartlett, G. J.; Sessions, R. B.; Brady, R. L.; Woolfson, D. N., Computational design of water-soluble alpha-helical barrels. *Science* **2014**, *346* (6208), 485-8.
67. Tian, Y.; Zhang, H. V.; Kiick, K. L.; Saven, J. G.; Pochan, D. J., Fabrication of One- and Two-Dimensional Gold Nanoparticle Arrays on Computationally Designed Self-Assembled Peptide Templates. *Chem. Mater.* **2018**, *30* (23), 8510-8520.
68. Tian, Y.; Polzer, F. B.; Zhang, H. V.; Kiick, K. L.; Saven, J. G.; Pochan, D. J., Nanotubes, Plates, and Needles: Pathway-Dependent Self-Assembly of Computationally Designed Peptides. *Biomacromolecules* **2018**, *19* (11), 4286-4298.
69. Tian, Y.; Zhang, H. V.; Kiick, K. L.; Saven, J. G.; Pochan, D. J., Transition from disordered aggregates to ordered lattices: kinetic control of the assembly of a computationally designed peptide. *Org. Biomol. Chem.* **2017**, *15* (29), 6109-6118.
70. Lanci, C. J.; MacDermaid, C. M.; Kang, S. G.; Acharya, R.; North, B.; Yang, X.; Qiu, X. J.; DeGrado, W. F.; Saven, J. G., Computational design of a protein crystal. *Proc. Natl. Acad. Sci. U. S. A.* **2012**, *109* (19), 7304-7309.

71. Calhoun, J. R.; Kono, H.; Lahr, S.; Wang, W.; DeGrado, W. F.; Saven, J. G., Computational design and characterization of a monomeric helical dinuclear metalloprotein. *J. Mol. Biol.* **2003**, *334* (5), 1101-1115.
72. Kono, H.; Saven, J. G., Statistical theory for protein combinatorial libraries. Packing interactions, backbone flexibility, and the sequence variability of a main-chain structure. *J. Mol. Biol.* **2001**, *306* (3), 607-628.
73. Cochran, F. V.; Wu, S. P.; Wang, W.; Nanda, V.; Saven, J. G.; Therien, M. J.; DeGrado, W. F., Computational de novo design and characterization of a four-helix bundle protein that selectively binds a nonbiological cofactor. *J. Am. Chem. Soc.* **2005**, *127* (5), 1346-1347.
74. MacKerell, A. D.; Bashford, D.; Bellott, M.; Dunbrack, R. L.; Evanseck, J. D.; Field, M. J.; Fischer, S.; Gao, J.; Guo, H.; Ha, S.; Joseph-McCarthy, D.; Kuchnir, L.; Kuczera, K.; Lau, F. T. K.; Mattos, C.; Michnick, S.; Ngo, T.; Nguyen, D. T.; Prodhom, B.; Reiher, W. E.; Roux, B.; Schlenkrich, M.; Smith, J. C.; Stote, R.; Straub, J.; Watanabe, M.; Wiorkiewicz-Kuczera, J.; Yin, D.; Karplus, M., All-atom empirical potential for molecular modeling and dynamics studies of proteins. *J. Phys. Chem. B* **1998**, *102* (18), 3586-3616.
75. Jorgensen, W. L.; Chandrasekhar, J.; Madura, J. D.; Impey, R. W.; Klein, M. L., COMPARISON OF SIMPLE POTENTIAL FUNCTIONS FOR SIMULATING LIQUID WATER. *J. Chem. Phys.* **1983**, *79* (2), 926-935.
76. Humphrey, W.; Dalke, A.; Schulten, K., VMD: Visual molecular dynamics. *J. Mol. Graphics Modell.* **1996**, *14* (1), 33-38.
77. Phillips, J. C.; Braun, R.; Wang, W.; Gumbart, J.; Tajkhorshid, E.; Villa, E.; Chipot, C.; Skeel, R. D.; Kale, L.; Schulten, K., Scalable molecular dynamics with NAMD. *J. Comput. Chem.* **2005**, *26* (16), 1781-1802.

78. Schuck, P., Size-distribution analysis of macromolecules by sedimentation velocity ultracentrifugation and Lamm equation modeling. *Biophys. J.* **2000**, *78* (3), 1606-1619.
79. Haider, M. J.; Zhang, H. V.; Sinha, N.; Fagan, J. A.; Kiick, K. L.; Saven, J. G.; Pochan, D. J., Self-assembly and soluble aggregate behavior of computationally designed coiled-coil peptide bundles. *Soft Matter* **2018**, *14* (26), 5488-5496.
80. Doucet, M.; Cho, J. H.; Alina, G.; Bakker, J.; Bouwman, W.; Butler, P.; Campbell, K.; Gonzales, M.; Heenan, R.; Jackson, A.; Juhas, P.; King, S.; Kienzle, P.; Krzywon, J.; Markvardsen, A.; Nielsen, T.; O'Driscoll, L.; Potrzebowski, W.; Ferraz Leal, R.; Richter, T.; Rozycko, P.; Snow, T.; Washington, A. *SasView version 4.2*, 4.2.0; Zenodo: 2018.
81. Zhu, Y. J.; Fu, X. R.; Wang, T.; Tamura, A.; Takada, S.; Saven, J. G.; Gai, F., Guiding the search for a protein's maximum rate of folding. *Chem. Phys.* **2004**, *307* (2-3), 99-109.
82. Bunagan, M. R.; Yang, X.; Saven, J. G.; Gai, F., Ultrafast folding of a computationally designed Trp-cage mutant: Trp(2)-cage. *J. Phys. Chem. B* **2006**, *110* (8), 3759-3763.
83. Jurrus, E.; Engel, D.; Star, K.; Monson, K.; Brandi, J.; Felberg, L. E.; Brookes, D. H.; Wilson, L.; Chen, J. H.; Liles, K.; Chun, M. J.; Li, P.; Gohara, D. W.; Dolinsky, T.; Konecny, R.; Koes, D. R.; Nielsen, J. E.; Head-Gordon, T.; Geng, W. H.; Krasny, R.; Wei, G. W.; Holst, M. J.; McCammon, J. A.; Baker, N. A., Improvements to the APBS biomolecular solvation software suite. *Protein Sci.* **2018**, *27* (1), 112-128.
84. Bottcher, A.; Kowerko, D.; Sigel, R. K. O., Explicit analytic equations for multimolecular thermal melting curves. *Biophys. Chem.* **2015**, *202*, 32-39.
85. Towns, J.; Cockerill, T.; Dahan, M.; Foster, I.; Gauthier, K.; Grimshaw, A.; Hazlewood, V.; Lathrop, S.; Lifka, D.; Peterson, G. D.; Roskies, R.; Scott, J. R.; Wilkins-Diehr, N., XSEDE: Accelerating Scientific Discovery. *Comput. Sci. Eng.* **2014**, *16* (5), 62-74.

Table of Contents image

